

¹ **An Autonomous Receiver/Digital Signal Processor**
² **Applied to Ground-Based and Rocket-Borne Wave**
³ **Experiments**

M. P. Dombrowski, J. LaBelle, D. G. McGaw, M. C. Broughton

4 **Abstract.** The programmable combined receiver/digital signal proces-
5 sor (Rx-DSP) platform presented in this article is designed for digital down-
6 sampling and processing of general waveform inputs with a 66 MHz initial

M. P. Dombrowski, Department of Physics and Astronomy, Dartmouth College, Room 315, 6127 Wilder Laboratory, Hanover, NH 03755, USA. (mpd@dartmouth.edu)

J. LaBelle, Department of Physics and Astronomy, Dartmouth College, Room 336, 6127 Wilder Laboratory, Hanover, NH 03755, USA. (jlabelle@aristotle.dartmouth.edu)

D. G. McGaw, Department of Physics and Astronomy, Dartmouth College, Room 316, 6127 Wilder Laboratory, Hanover, NH 03755, USA. (david.g.mcgaw@dartmouth.edu)

M. C. Broughton, Department of Physics and Astronomy, Dartmouth College, Room 336, 6127 Wilder Laboratory, Hanover, NH 03755, USA. (matbroughton0@gmail.com)

¹Department of Physics and Astronomy,
Dartmouth College

7 sampling rate and multi-input synchronized sampling. Systems based on this
8 platform are capable of fully autonomous low-power operation, can be pro-
9 grammed to preprocess and filter the data for preselection and reduction, and
10 may output to a diverse array of transmission or telemetry media. We de-
11 scribe three versions of this system, one for deployment on sounding rock-
12 ets and two for ground-based applications. The rocket system was flown on
13 the CHARM-II mission launched from Poker Flat Research Range, Alaska,
14 in 2010. It measured auroral ‘roar’ signals at 2.60 MHz. The ground-based
15 systems have been deployed at Sondrestrom, Greenland and South Pole Sta-
16 tion, Antarctica. The Greenland system synchronously samples signals from
17 three spaced antennas providing direction finding of 0-5 MHz waves. It has
18 successfully measured auroral signals and man-made broadcast signals. The
19 South Pole system synchronously samples signals from two crossed anten-
20 nas, providing polarization information. It has successfully measured the po-
21 larization of AKR-like signals as well as auroral hiss. Further systems are in
22 development for future rocket missions and for installation in Antarctic Au-
23 tomatic Geophysical Observatories.

1. Introduction

24 Instabilities in space plasmas produce waves in a wide range of frequencies
25 and bandwidths, with a large variety of time signatures, detectable both in
26 situ and remotely. Detector technologies include inductive loops for magnetic
27 fields, double probes for electric fields, and Langmuir probes for plasma den-
28 sity. For receivers, the ideal wave analysis instrument would involve a direct
29 high-frequency analog-to-digital (ADC) sampling of the output of a given
30 detector or antenna, with the highest possible sampling rate and bit depth.
31 While technology has advanced in recent years to allow continuous sampling
32 at 20 MHz or beyond, it is often not feasible to use such techniques directly,
33 due to limited data transmission and storage capabilities.

34 Furthermore, it is often desirable to record wave data from multiple de-
35 tectors simultaneously, e.g. from spatially separated or orthogonal antennae.
36 Such measurements can allow detection of wave polarization and propaga-
37 tion directions. Simultaneous sampling requires a high degree of ADC sample
38 synchronization across multiple receivers, and results in even greater demands
39 on data storage and transmission systems, rendering direct simultaneous sam-
40 pling even less attractive.

41 Data storage and transmission limitations are at their most severe on space-
42 craft, and therefore many innovative solutions have come out of that commu-
43 nity. For example, the Cluster satellites, launched in 2000, included the Wide-
44 Band plasma investigation (WBD). This instrument was capable of downcon-
45 verting in selected frequency bands, removing the need for storage of samples
46 at twice the Nyquist rate [*Gurnett et al.*, 1997]. Another example is the Waves
47 instrument onboard the Van Allen Probes (formerly RBSP), launched August
48 2012, which is similar to the WBD, but also allows for dynamic Fast Fourier
49 Transforms (FFTs) and data compression [*Kletzing et al.*, 2013]. The receiv-
50 ing system most similar to the subject of this paper is the Radio Receiver
51 Instrument (RRI) on board the e-POP payload of the Canadian CASSIOPE
52 satellite. The RRI directly samples four probes at 40 MHz and then performs
53 on-board signal processing [*James et al.*, 2015].

54 The Dartmouth Receiver/Digital Signal Processor (Rx-DSP) represents an-
55 other recent development effort to address these issues. As a digital down-
56 sampling receiver, it can transmit wave data within a specific band or set of
57 bands within the 0 to 33 MHz range. The data can be sampled either continu-
58 ously or in bursts, allowing for fine-grained customization of the transmission
59 data rate. In addition, the Rx-DSP boards are designed for cross-receiver
60 sample synchronization to within 2 nanoseconds. The Rx-DSP is set apart

61 by its autonomous capabilities with remote reprogrammability, high maxi-
62 mum sample rate, and myriad options for data transmission. The generalized
63 nature of the instrument front-end allows for use with a wide range of de-
64 tector hardware. It also allows for a variety of both spacecraft-borne and
65 ground-based applications, as discussed below.

66 Section 2, describes the current iteration of the Dartmouth Rx-DSP hard-
67 ware, and Section 3 explains the naming convention for individual deploy-
68 ments. Section 4 provides an overview of the firmware used on the onboard
69 programmable DSP. Finally, Section 5 presents three examples of applica-
70 tions of this system to space physics, with case studies of one rocket mission
71 and two ground-based detectors.

2. Hardware

72 The Rx-DSP is a low-cost analog-to-digital receiver and signal processor
73 board, designed for use in both ground and space scenarios, and specifi-
74 cally engineered for cross-board sample-synchronized acquisition. The use
75 of purpose-specific receiver components allows for a significant shortening
76 of system development cycles as compared to an FPGA-based solution, by
77 removing programming, testing, and debugging complexities; however, the
78 specific components chosen for the Rx-DSP platform maintain appreciable
79 flexibility in the field. The detailed architecture of the boards has sounding

80 rocket flight history from instruments produced at the University of Iowa.
81 The current generation of boards have been tested for reliable operation at
82 temperatures from 0 to 50 C—more extreme ground environments require
83 external regulation, such as placement in insulated or heated boxes, whereas
84 sounding rockets are warmed on the launch pad, and flights are not long
85 enough for cooling to be a concern. While the Rx-DSP design could be ex-
86 tended for high-radiation space environments, this has not been a goal of
87 current development efforts. Data acquisition systems incorporating the Rx-
88 DSP are easily crafted for autonomous operation with no external command
89 and control, transmitting results via a number of protocols. Figure 1 shows a
90 picture of the topmost Rx-DSP board in a stack of two—a configuration used
91 in several applications. The data flows through the board as in Figure 2,
92 going through asynchronous Receive, Processing, and Transmit stages.

93 The Receive stage takes a balanced analog signal with a maximum 1 volt
94 peak-to-peak amplitude, fed to the input of an Analog Devices AD6644 ADC,
95 which samples at 66.6666 MHz with 14-bit resolution, yielding a 33.3333 MHz
96 Nyquist frequency, 74 dB signal-to-noise ratio (SNR), and 100 dB spurious-
97 free dynamic range. There is no built-in filtering, and an input bandwidth of
98 250 MHz, allowing for undersampling downconversion; thus, each application
99 requires customized front-end pre-amplifiers and filters for band-limiting and

100 antialiasing. The outputs of the 6644 are linked directly to an Analog Devices
101 AD6620 programmable digital Receive Signal Processor (RSP). This processor
102 performs quadrature frequency translation, and then decimates and filters the
103 incoming signal through three stages, yielding a band with width, center, and
104 filter characteristics defined by a table of values and filter coefficients. The
105 RSP can further improve the SNR, and the total system performance and
106 frequency response will be unique to each application, determined by the
107 preamplifiers, filters, and cabling used. The quadrature data is output from
108 the RSP as 16-bit words, with In-phase and Quadrature (I and Q) words being
109 interleaved, and each word is accompanied by a bit which indicates whether
110 a given sample is an I or Q word. This relatively low-frequency, 17-bit data
111 is then stored to an 18-bit Integrated Device Technology IDT72285 First-In
112 First-Out (FIFO) buffer.

113 The receive FIFO output is accessible to a Texas Instruments (TI)
114 TMS320C542 Digital Signal Processor. This processor has a number of use-
115 ful built-in peripherals, runs on an external clock (generally set for 40 MHz
116 operation), has 10 kilowords of built-in RAM, and can access up to 16 KB of
117 program code and tables from an external PROM. In many deployments, this
118 DSP acts only as a data router and packager, adding headers and/or synchro-
119 nization information before passing the data onwards. However, by loading

120 custom software to this processor, a variety of real-time, streaming data pro-
121 cessing effects are achievable, such as FFTs and various types of compression,
122 though no such deployments will be shown in the case-studies herein.

123 After all desired data processing steps are complete, the data in memory
124 can follow a number of output paths. First, the data can be sent at high
125 speed to a second IDT72285 FIFO. The outputs of this FIFO are accessible
126 to high-speed serial and parallel LVDS outputs, at any speed up to the full
127 quadrature data rate. A second option can exploit one of two serial ports
128 available on the TMS320C542: a buffered serial port that allows efficient data
129 transfer at standard RS-232 speeds, and a time-division multiplexed port that
130 allows multiple boards to share one serial link. A third option makes use of
131 a parallel Host Port Interface that allows the DSP to connect to an external
132 device at high speeds (up to 8 MBps). Finally, a fourth possibility is to
133 wire and program the Rx-DSP to allow dropping to a single-line interactive
134 serial console, through which a user can trigger single acquisitions, read data,
135 configure settings, or remotely re-burn the firmware EEPROM.

136 In many use cases, the DSP is able to spend idle time in a low-power mode,
137 significantly reducing the average power draw of the Rx-DSP board—without
138 detailed optimization, the power draw per Rx-DSP is approximately 1.5 W.
139 The flexibility in configuration, coding, and data output allow for a wide

140 range of receiver setups. In addition, the AD6620 is designed to allow for
141 sample synchronization across chips, and the Rx-DSP boards are designed
142 to allow the sample clocks and RSPs to be synchronized as well, using short
143 (< 10 cm) jumper wires which pass the clock and AD6620 synchronization
144 lines between boards. This allows for the development of multi-board setups
145 for wave-polarization measurements and direction finding.

3. Nomenclature

146 Each individual deployment of Rx-DSP hardware requires custom hardware
147 for input refinement, power, command input, and data output. For ease of
148 referral, each Rx-DSP system may be referred to as an **A**utonomous **R**x-DSP
149 **C**luster (ARC), with a prefix signifying current data collection intent. The
150 current set of prefixes are arrayed below:

- 151 1. P - Polarization
- 152 2. F - Fine Structure
- 153 3. M - Multi-Band
- 154 4. I - Imaging/Direction-Finding
- 155 5. S - Spectrum Analyzing

156 The other element which is generally different in each ARC is the firmware
157 loaded by the TMS320C542 processor.

4. Firmware Overview

158 The limited RAM on the TMS320C542 processor is shared between loaded
159 programs and data, requiring careful management of program size and data
160 storage. The programs used are all hand-coded in TI DSP Assembly, except
161 for the FFT module, which is based on code from the TI DSP C Library. The
162 default mode upon power-up has the DSP load its program code from the
163 onboard PROM and then commence execution.

164 The program code developed at Dartmouth for rocket and ground-based
165 application is modular, but all implementations follow a general structure
166 outlined in Figure 3. After initializing the C542 and AD6620 hardware, the
167 AD6620 acquisition is started, and data is loaded into RAM by the C542.
168 For continuous high-speed data acquisition, the AD6620 may be left ‘on’;
169 however, when only discrete data blocks are required, power usage can be cut
170 significantly by halting acquisition between blocks.

171 Once the data is in RAM, any number of processing steps can apply, lim-
172 ited only by available RAM and processing time. In the simplest case the
173 data is untouched. In the most complex case currently coded, 1024-word
174 FFTs are performed on incoming data. For most cases, the data is next
175 encapsulated in a synchronization framework, which includes sync words,

176 sampling-specification headers, and frame counters. The processed data is
177 next prepared for output.

178 Data handling for output varies widely, depending on final destination, DSP
179 setup, and output hardware. To output to the high-speed serial or parallel
180 systems, data is merely copied into the output FIFO and then read out via
181 rocket telemetry or PC USB hardware. For output involving the C542 chip's
182 built-in peripherals, various preprocessing steps may be required, including
183 downsampling, data subset selection, endianness conversion, and the addition
184 of extra sync data and headers. The most efficient C542 peripheral for data
185 output is the Buffered Serial Port, which merely requires that its rotating
186 buffer is periodically filled. All other peripherals require that each byte be
187 individually preloaded. In either case, data loading can either be handled by
188 fixed software loops, or can be interrupt driven.

189 A special case for input and output on the DSP is the software serial console
190 interface. This link allows a PC with a standard RS-232 serial port to connect
191 to the C542, which can be switched into the serial console mode via an external
192 toggle. The console allows for single acquisitions, direct editing of program
193 code in RAM, modifications to the AD6620 setup, and for the uploading and
194 burning of new PROM files for permanent changes.

5. Case Studies

5.1. CHARM-II — Rocket-Borne Application

195 Auroral roar is a natural ionospheric radio emission characterized by a rel-
196 atively narrow-banded structure centered at frequencies near multiples of the
197 electron cyclotron frequency. It is most frequently observed by ground-based
198 radio receivers, but has also been seen by satellites [*James et al.*, 1974; *Ben-*
199 *son and Wong*, 1987; *Bale*, 1999]. The intense electrostatic upper-hybrid
200 waves which are the source of auroral roar have been detected by a sounding
201 rocket, but hitherto not the auroral roar itself [*Samara et al.*, 2004]. De-
202 tailed ground-based studies have shown that many instances of roar are not
203 singular emissions, but rather contain intricate fine structures visible on high-
204 resolution frequency-time plots [*LaBelle et al.*, 1995; *Shepherd et al.*, 1998b].
205 Further studies have determined that the lowest harmonic of roar seen on
206 the ground ($2f_{ce}$) is left-hand elliptically polarized with respect to the local
207 magnetic field [*Shepherd et al.*, 1997], while there have been observations of
208 higher harmonics being either left or right-hand polarized [*Sato et al.*, 2012].
209 It is theorized that roar originates as upper-hybrid plasma waves above the
210 ionospheric ‘F peak’, converting through linear or nonlinear processes into
211 propagating electromagnetic waves [*Shepherd et al.*, 1998a; *Yoon et al.*, 2000;

212 *Ye et al.*, 2007], and the HIBAR and Porcupine sounding rockets may have
213 encountered regions of such plasma waves [*Carlson et al.*, 1987].

214 The Correlation of High-Frequency and Auroral Roar Measurements
215 (CHARM-II) auroral sounding rocket carried the second successful deploy-
216 ment of the Rx-DSP hardware. On the CHARM-I mission the Rx-DSPs
217 returned approximately 1-2 minutes of data from exposed, partially deployed
218 electric-field probes, before these probes sheared off due to catastrophic pay-
219 load failure. The CHARM-II mission was launched from the Poker Flat Re-
220 search Range near Fairbanks, AK, at 9:49 UT/22:46 MLT on 16 February
221 2010, reaching an apogee of 802 km. The payload carried a two-board FP-
222 ARC, each receiver digitizing the differential voltage between two 2.5 cm
223 spherical aluminum probes, with the two probe sets positioned perpendic-
224 ular to each other in the plane orthogonal to the rocket's spin axis, which
225 was oriented parallel to the geomagnetic field. The Rx-DSPs were in a sim-
226 ple downsampling mode, adding short headers and outputting through the
227 high-speed telemetry FIFO and LVDS serial link. The data rate was set to
228 maximally utilize two S-band telemetry links, transmitting downsampled data
229 in a 333 kHz band centered at 2.67 MHz. As the payload nominally had its
230 spin axis aligned with the Earth's magnetic field, B , the Rx-DSPs in this con-

231 figuration effectively yielded a picture of the projection of electric-field wave
 232 activity onto the plane perpendicular to B within the designated band.

233 The CHARM-II FP-ARC yielded the first in-situ observation of auroral
 234 roar with both high time resolution and polarization data. Figure 4 shows
 235 spectrograms over a 298 to 330 kHz band from 771 to 777 seconds after launch,
 236 corresponding to 548 to 536 km altitude on the downleg of the flight. The
 237 color scale represents the power of righthand circularly polarized signals (a)
 238 and lefthand circularly polarized signals (b), with polarizations being with
 239 respect to B .

Figure 4 was generated using a technique described by *LaBelle and Treumann* [1992], adapted from *Kodera et al.* [1977]. Given time series data corresponding to two perpendicular, transverse components of a field, as from the measured X and Y components from the Rx-DSPs, a spectral power can be estimated for lefthand and righthand circular wave polarization by recombining the complex Fast Fourier Transforms (FFT) of the time series, according to

$$\begin{aligned} FFT_L &= FFT_X + i \times FFT_Y, \\ \text{and } FFT_R &= FFT_X - i \times FFT_Y. \end{aligned}$$

240 For the CHARM II data, the two perpendicular quadrature signals are de-
 241 tected in situ, and transmitted to ground via payload telemetry systems. In

242 post-flight processing, the data is FFTed, and then recombined to yield the
243 estimated left and righthand powers shown in Figure 4.

244 Figure 4 clearly establishes that the observed waves are lefthand polarized.
245 Not only does this confirm the ground-level observations of *Shepherd et al.*
246 [1997], it expands upon it, as the high time and frequency resolution makes it
247 clear that the individual fine structures are all lefthand polarized. *Sato et al.*
248 [2015] have performed a similar analysis for ground-level $4f_{ce}$ roar emissions.
249 The lefthand polarization of these waves is consistent with various generation
250 theories, especially those put forth by *Yoon et al.* [2000].

5.2. South Pole Station — Ground-Based Application

251 South Pole Station (SPS) lies on the Antarctic Plateau thousands of kilo-
252 meters from commercial and other broadcast activities associated with pop-
253 ulation centers. As a result, the station is very favorable for studies of radio
254 emissions of natural origin, and hosts a variety of radio receivers at ELF to
255 HF frequencies, complemented by other geophysical diagnostics such as all-sky
256 cameras, photometers, and flux-gate magnetometers. Significant observations
257 at VLF [*Martin*, 1960; *Chevalier et al.*, 2007], LF-MF [*LaBelle et al.*, 2005;
258 *Ye et al.*, 2006; *Yan et al.*, 2013; *Broughton et al.*, 2014], and HF [*Rodger and*
259 *Rosenberg*, 1999; *Patterson et al.*, 2001] have been made at the station.

260 Hence, it was a natural decision to deploy the Rx-DSP to the South Pole.
261 In January 2012 Dartmouth installed a PF-ARC at SPS, consisting of two
262 Rx-DSP boards wired to perform synchronized sampling. Two 40 m^2 loop
263 antennas perpendicular to each other, supported by a 10 m mast, were con-
264 structed about 1 km from the station. Figure 5a shows these antennas. The
265 planes of the loops are perpendicular to the ground and to each other, pro-
266 viding highest sensitivity to waves coming from overhead, and allowing right-
267 and left-hand polarization to easily be distinguished from the phase relation
268 between the signals. The ARC, a duplicate of that shown in Figure 5b was
269 programmed for continuous sampling of a 330-kHz band centered on 515 kHz.
270 Data were offloaded to a PC through the Rx-DSP parallel LVDS link via a
271 pair of QuickUSB high-speed USB data acquisition modules, and stored on
272 an array of 2 TB hard drives. Spectral and cross-spectral analysis of the sig-
273 nals on the Linux computer determined power and polarization of all signals
274 exceeding the noise level. All computer hardware as well as the ARC were
275 housed in an insulated box as in Figure 5c, designed to retain waste heat,
276 keeping them within their operating temperature range after installation in
277 the unheated V8 science vault at SPS.

278 Figure 6 shows spectrograms recorded by this ARC on two days in 2013:
279 July 8 and August 2. In both cases, five minutes of data from one of the

280 two signals are shown, and the data come from within 1.5 hours of magnetic
281 midnight, which occurs at 03:35 UT at South Pole. In both spectrograms,
282 sharp decreases in the signal power spectral density near the band edges
283 show the effectiveness of the digital filtering in the RX-DSP which defines
284 the bandwidth. Despite the remoteness of South Pole Station, activities at
285 the station lead to strong interference lines, most prominently at 450-460 kHz
286 and 640-650 kHz in each spectrogram and somewhat more weakly at 570-580
287 kHz and 420-430 kHz.

288 However, between these interference lines, both spectrograms show evidence
289 of natural radio emissions of auroral origin. The bottom panel, from July 8,
290 2013, shows a phenomenon called auroral hiss [*Makita, 1979; Sazhin et al.,*
291 *1993; LaBelle and Treumann, 2002*]. The high resolution Rx-DSP data show
292 that at LF the hiss consists of impulsive emissions appearing as vertical lines
293 on the spectrogram.

294 The top panel, from August 2, 2013, shows a phenomenon called ‘AKR-like
295 emissions’ [*LaBelle and Anderson, 2011; LaBelle et al., 2015*]. This phe-
296 nomenon is characterized by complicated fine frequency structure consisting
297 of rising and falling tones with typical slopes of hundreds of Hz per second.
298 These features qualitatively resemble those observed in outgoing X-mode au-
299 roral kilometric radiation (AKR) detected with satellite-borne receivers at

300 great distances from Earth [*Gurnett and Anderson, 1981*]. As pointed out by
301 *LaBelle et al. [2015]*, the strong resemblance between this phenomenon and
302 AKR, combined with the stark differences between it and the auroral hiss
303 shown in the top panel of Figure 6, forms a powerful argument for a con-
304 nection between the ground-level AKR-like emissions and the outgoing AKR
305 observed in space.

306 Due to the success of these observations, further experiments are planned
307 with the Rx-DSP at South Pole. For example, in Summer-Fall 2014 and Sum-
308 mer 2015, the South Pole ARC was operated during anticipated conjunctions
309 between it and Cluster satellites, with the Cluster wave instrument tuned
310 to the same frequency band, in hopes of detecting identical fine structure in
311 ground and in space. Furthermore, as described above, an S-ARC which can
312 perform live spectrum analysis is being installed in Automatic Geophysical
313 Observatories. These autonomous digital receivers in the low-noise Antarc-
314 tic environment show promise to make important advances in understanding
315 radio waves of auroral origin.

5.3. Sondrestrom Research Facility — Ground-Based Application

316 The Sondrestrom Research Facility lies on the southwest coast of Greenland
317 near Kangerlussuaq, at 66.99° N 309.06° E and is home to numerous instru-
318 ments for researching Earth's upper atmosphere. These include an incoherent

319 scatter radar, allsky imagers, riometers, magnetometers, and various radio re-
320 ceivers. The MI-ARC at this site consists of a trio of sample-synchronized
321 Rx-DSPs. Input to these comes from five loop antennae: one reference, two
322 situated 50 m from this along lines perpendicular to each other, and two more
323 at 400 m from reference along the same lines. The antennas are arrayed in
324 a small valley approximately 1 km from the station. The three-board MI-
325 ARC is installed in an unheated vault next to the reference antenna, with
326 the receiver itself in a heated, insulated box. The only connection from the
327 vault to the station is a single coaxial cable, which carries both the serial
328 digital output of the ARC, and DC voltage that powers the ARC. The entire
329 array is calibrated at installation and after any major system changes or re-
330 pairs, through observation of analog reference signals with known strengths
331 and physical source positions.

332 The ARC triggers relays to switch between the 50 m and 400 m antenna
333 pairs when digitizing signals above and below 1 MHz, respectively. The DSPs
334 are set for discrete sampling of 750 kHz bands, with the receivers rotating
335 through a set of four center frequencies (475, 1225, 1975, and 2725 kHz)
336 approximately once per second. The data are offloaded through the buffered
337 serial port, interleaved via a hardware serial multiplexer, and then transmitted
338 via RS-232 serial link to a remote PC.

339 To compute the direction of arrival for incoming signals, the three resultant
340 data streams are combined pairwise through cross-spectrum analysis, and
341 averaged over eight 128 or 512-bin FFT ensembles. Then, given calibration
342 data and knowledge of the antenna layout and cable lengths, the phase delays
343 of the resulting spectra can be used to calculate the direction of arrival of
344 high-coherence signals.

345 Figure 7 shows an example of such an analysis for 14 Sep 2013, using sig-
346 nals from 1-1.5 MHz with coherence greater than 0.95. The scatter plot above
347 shows elevation vs. azimuth for over 10,000 signals, where elevation is degrees
348 off the horizon and azimuth is degrees from true north. Note that various in-
349 strumental uncertainties yield about a 5% uncertainty for each point. The ac-
350 companying map shows the approximate azimuthal extent of the two clusters
351 of points. It is clear that the signals detected originate from the directions of
352 North America and Europe. One curiosity is the extension of North American
353 signals to lower elevations, which implies sensitivity to more distant signals.
354 This may be due to atmospheric inhomogeneities or field-of-view anisotropy.

355 These results establish that the Sondrestrom receiver array/MI-ARC pro-
356 duces accurate direction finding with high time and frequency resolution. The
357 system is resource-efficient, operating autonomously and remotely via a single
358 1 km coaxial data/power cable.

6. Summary

359 The Rx-DSP is a flexible platform for high-frequency geophysical data ac-
360 quisition. ARCs are able to be crafted for autonomous operation in extremely
361 remote regions, for low power draw, and for a wide variety of data transmis-
362 sion rates and media. In particular, the potential for on-board data analysis,
363 reduction, selection, and compression allows for optimal use of low-bandwidth
364 telemetry systems. Additional deployments are already underway, and future
365 revisions of this platform should allow for even more diverse uses.

366 **Acknowledgments.** Thanks to J. C. Vandiver for hardware and firmware
367 development and maintenance, and to Spencer Hatch for presenting this in-
368 strument at the 2015 Conference on Measurement Techniques in Solar and
369 Space Physics.

370 The data discussed may be acquired by contacting Jim LaBelle
371 (jlabelle@aristotle.dartmouth.edu). Work supported by NASA grant
372 NNX12AI44G and NSF grants ANT-1141817 and PLR-1443338.

References

373 Bale, S. D., Observation of topside ionospheric mf/hf radio emission from
374 space, *Geophys. Res. Lett.*, 26(6), 667–670, 1999.

- 375 Benson, R. F., and H. K. Wong, Low-altitude isis 1 observations of auroral
376 radio emissions and their significance to the cyclotron maser instability, *J.*
377 *Geophys. Res.*, *92*(A2), 1218–1230, 1987.
- 378 Broughton, M. C., J. LaBelle, and P. H. Yoon, A new natural radio emission
379 observed at south pole station, *J. Geophys. Res.*, *119*(1), 566–574, doi:
380 10.1002/2013JA019467, 2014.
- 381 Carlson, C. W., R. E. Ergun, A. J. Mallinckrodt, and G. Haerendel, Obser-
382 vations of intense electron Bernstein wave emissions in an auroral plasma
383 (unpublished manuscript), 1987.
- 384 Chevalier, M. W., W. B. Peter, U. S. Inan, T. F. Bell, and M. Spasojevic, Re-
385 mote sensing of ionospheric disturbances associated with energetic particle
386 precipitation using the south pole vlf beacon, *J. Geophys. Res.*, *112*(A11),
387 11,306, doi:10.1029/2007JA012425, 2007.
- 388 Gurnett, D. A., and R. R. Anderson, *The Kilometric Radio Emission Spec-*
389 *trum: Relationship to Auroral Acceleration Processes*, *Geophysical Mono-*
390 *graph*, vol. Physics of Auroral Arc Formation, AGU, 1981.
- 391 Gurnett, D. A., R. L. Huff, and D. L. Kirchner, The wide-band plasma wave
392 investigation, *Space Sci. Rev.*, *79*, 195–208, 1997.
- 393 James, H. G., E. L. Hagg, and L. P. Strange, Narrowband radio noise in the
394 topside ionosphere, in *Non-Linear Effects in Electromagnetic Wave Prop-*

395 *agation*, no. 138 in Conference Pre-Prints, North Atlantic Treaty Orga-
396 nization, Advisory Group for Aerospace Research & Development, 7 Rue
397 Ancelle, 92200, Neuilly Sur Seine, France, 1974.

398 James, H. G., E. P. King, A. White, R. H. Hum, W. H. H. L. Lunscher, and
399 C. L. Siefring, The e-pop radio receiver instrument on cassiope, *Space Sci.*
400 *Rev.*, 2015.

401 Kletzing, C. A., W. S. Kurth, M. Acuna, R. J. MacDowall, R. B. Tor-
402 bert, T. Averkamp, D. Bodet, S. R. Bounds, M. Chutter, J. Connerney,
403 D. Crawford, J. S. Dolan, R. Dvorsky, G. B. Hospodarsky, J. Howard,
404 V. Jordanova, R. A. Johnson, D. L. Kirchner, B. Mokrzycki, G. Needell,
405 J. Odom, D. Mark, J. R. F. Pfaff, J. R. Phillips, C. W. Piker, S. L. Rem-
406 ington, D. Rowland, O. Santolik, R. Schnurr, D. Sheppard, C. W. Smith,
407 R. M. Thorne, and J. Tyler, The electric and magnetic field instrument
408 suite and integrated science (emfisis) on rbsp, *Space Sci. Rev.*, 179, 127–
409 181, doi:10.1007/s11214-013-9993-6, 2013.

410 Kodera, K., R. Gendrin, and C. de Villedary, Complex representation of a
411 polarized signal and its application to the analysis of ulf waves, *J. Geophys.*
412 *Res.*, 82(7), 1245–1255, 1977.

413 LaBelle, J., and R. R. Anderson, Ground-level detection of auroral kilometric
414 radiation, *Geophys. Res. Lett.*, 38(4), doi:10.1029/2010GL046411, 2011.

- 415 LaBelle, J., and R. A. Treumann, Poynting vector measurements of electro-
416 magnetic ion cyclotron waves in the plasmasphere, *J. Geophys. Res.*, *97*
417 (*A9*)(13), 789–797, 1992.
- 418 LaBelle, J., and R. A. Treumann, Auroral radio emissions, 1. hisses, roars,
419 and bursts, *SSR*, *101*(3, 4), 295–440, 2002.
- 420 LaBelle, J., M. L. Trimpi, R. Brittain, and A. T. Weatherwax, Fine structure
421 of auroral roar emissions, *J. Geophys. Res.*, *100*(A11), 21,953–21,959, 1995.
- 422 LaBelle, J., A. T. Weatherwax, M. Tantiwiwat, E. Jackson, and J. Linder,
423 Statistical studies of auroral mf burst emissions observed at south pole
424 station and at multiple sites in northern canada, *J. Geophys. Res.*, *110*(A2),
425 doi:10.1029/2004JA010608, 2005.
- 426 LaBelle, J., X. Yan, M. C. Broughton, S. Pasternak, M. P. Dombrowski,
427 R. R. Anderson, H. U. Frey, A. T. Weatherwax, and Y. Ebihara, Further
428 evidence for a connection between auroral kilometric radiation and ground-
429 level signals measured in antarctica, *J. Geophys. Res.*, *120*(3), 2061–2075,
430 doi:10.1002/2014JA020977, 2015.
- 431 Makita, K., *VLF-LF Hiss Emissions Associated with Aurora*, *Memoirs of*
432 *National Institute of Polar Research: Aeronomy*, vol. 16, National Institute
433 of Polar Research, 1979.

- 434 Martin, L. H., Observations of ‘whistlers’ and ‘chorus’ at the south pole,
435 *Nature*, *187*, 1018–1019, doi:10.1038/1871018a0, 1960.
- 436 Patterson, J. D., T. P. Armstrong, C. M. Laird, D. L. Detrick, and A. T.
437 Weatherwax, Correlation of solar energetic protons and polar cap absorp-
438 tion, *J. Geophys. Res.*, *106*(A1), 149–163, doi:10.1029/2000JA002006, 2001.
- 439 Rodger, A. S., and T. J. Rosenberg, Riometer and hf radar signatures of polar
440 patches, *Radio Science*, *34*(2), 501–508, doi:10.1029/1998RS900005, 1999.
- 441 Samara, M., J. LaBelle, C. A. Kletzing, and S. R. Bounds, Rocket observations
442 of structured upper hybrid waves at $f_{uh} = 2f_{ce}$, *Geophys. Res. Lett.*, *31*(22),
443 2004.
- 444 Sato, Y., T. Ono, N. Sato, and Y. Ogawa, First observations of $4f_{ce}$ auroral
445 roar emissions, *Geophys. Res. Lett.*, *39*(7), 2012.
- 446 Sato, Y., A. Kadokura, Y. Ogawa, A. Kumamoto, and Y. Katoh, Polarization
447 observations of $4f_{ce}$ auroral roar emissions, *Geophys. Res. Lett.*, *42*(2), 249–
448 255, 2015.
- 449 Sazhin, S. S., K. Bullough, and M. Hayakawa, Auroral hiss: a review, *Plane-*
450 *tary and Space Science*, *41*(2), 153–166, 1993.
- 451 Shepherd, S. G., J. LaBelle, and M. L. Trimpi, The polarization of auroral
452 radio emissions, *Geophys. Res. Lett.*, *24*(24), 3161–3164, 1997.

- 453 Shepherd, S. G., J. LaBelle, R. A. Doe, M. McCready, and A. T. Weatherwax,
454 Ionospheric structure and the generation of auroral roar, *J. Geophys. Res.*,
455 *103*(A12), 29,253–29,266, 1998a.
- 456 Shepherd, S. G., J. LaBelle, and M. L. Trimpi, Further investigation of auroral
457 roar fine structure, *J. Geophys. Res.*, *103*(A2), 2219–2229, 1998b.
- 458 Yan, X., J. LaBelle, G. Haerendel, M. Spasojevic, N. L. Bunch, D. I. Golden,
459 H. U. Frey, and A. T. Weatherwax, Dayside auroral hiss observed at south
460 pole station, *J. Geophys. Res.*, *118*(3), 1220–1230, doi:10.1002/jgra.50141,
461 2013.
- 462 Ye, S., J. LaBelle, and A. T. Weatherwax, Further study of flickering auroral
463 roar emission: 1. south pole observations, *J. Geophys. Res.*, *111*(A7), doi:
464 10.1029/2005JA011271, 2006.
- 465 Ye, S., J. LaBelle, P. H. Yoon, and A. T. Weatherwax, Experimental tests of
466 the eigenmode theory of auroral roar fine structure and its application to
467 remote sensing, *J. Geophys. Res.*, *112*(A12304), doi:10.1029/2007JA012525,
468 2007.
- 469 Yoon, P. H., A. T. Weatherwax, and J. LaBelle, Discrete electrostatic eigen-
470 modes associated with ionospheric density structure: Generation of auroral
471 roar fine frequency structure, *J. Geophys. Res.*, *105*(A12), 27,589–27,596,
472 2000.

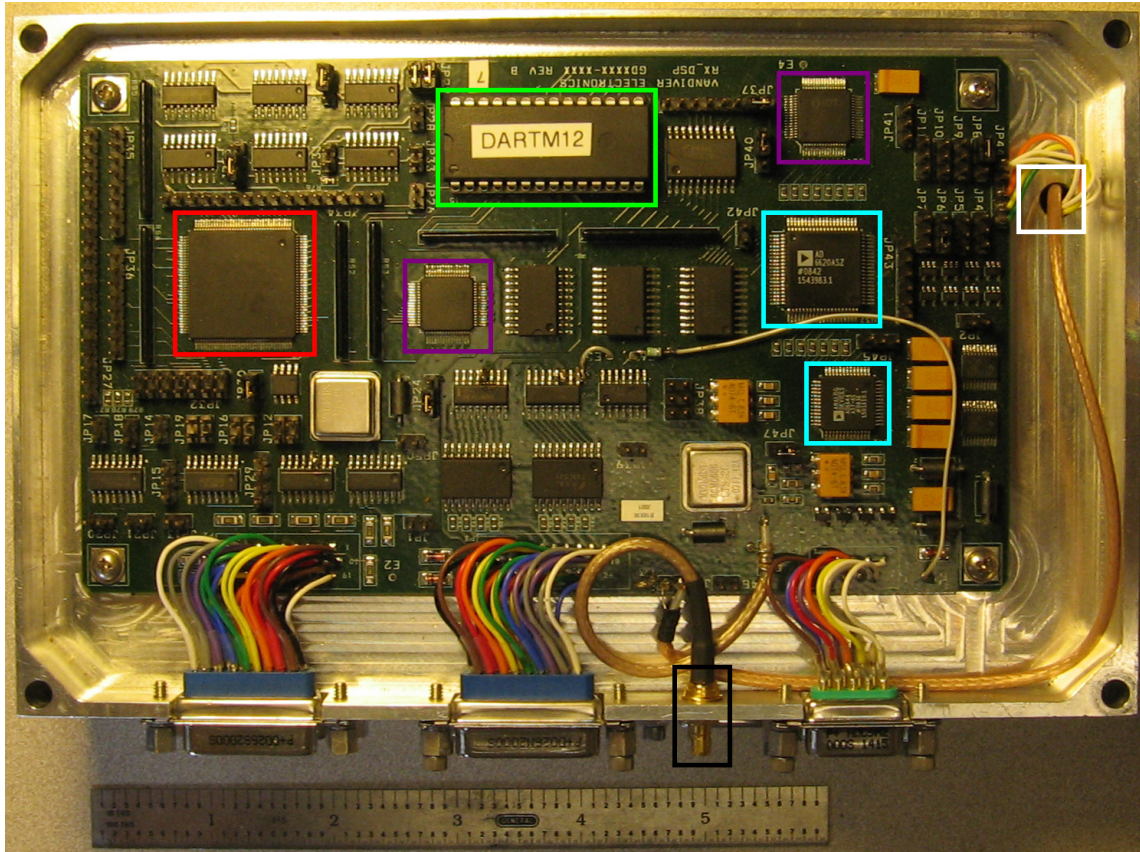


Figure 1. A photograph of the top board of an Rx-DSP stack ready for a rocket flight, with 6 inch ruler for scale. Highlighted are the SMB signal input (black), cross-board synchronization lines (white), AD6644 & AD6620 signal processors (cyan), IDT72285 FIFOs (purple) TMS320C542 programmable processor (red), and the program-code EEPROM (green).

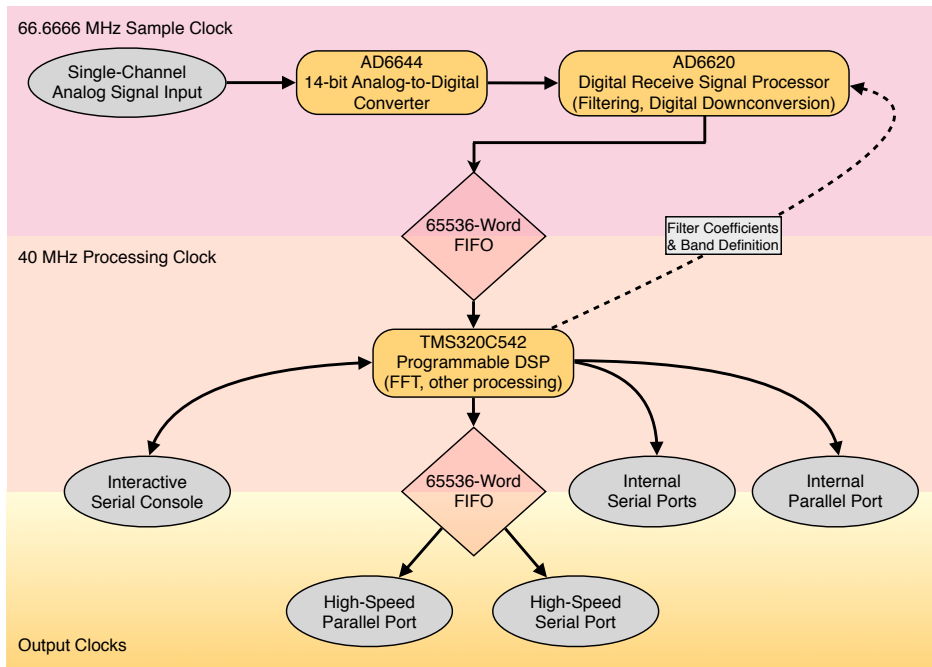


Figure 2. A diagram depicting the major parts of the Rx-DSP hardware, and the data flow between them, with the dashed line indicating command/control and solid lines indicating data or both. The colored background boxes indicate which systems are controlled by which clocks.

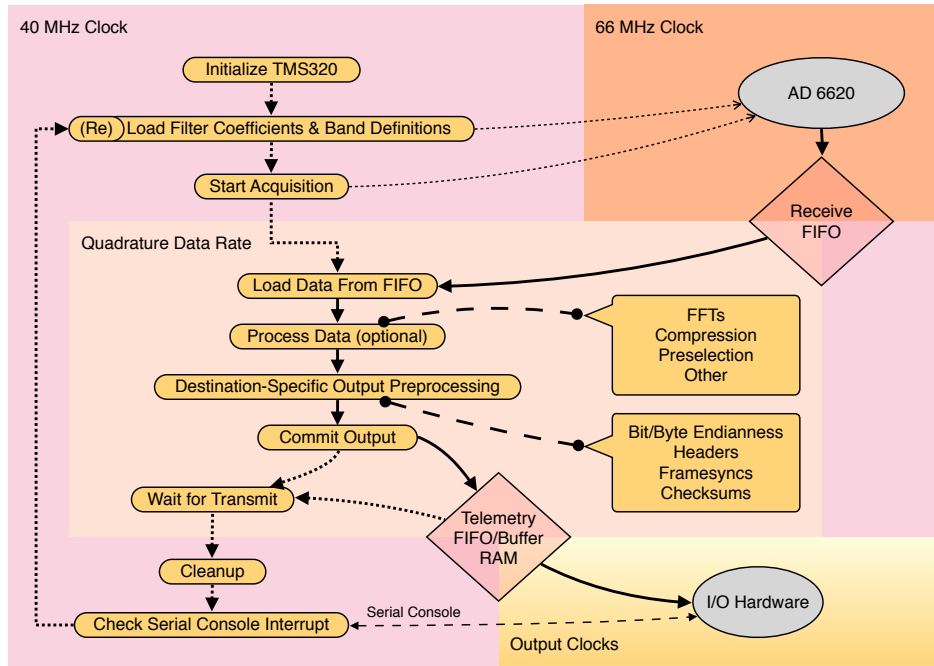


Figure 3. A diagram depicting a generalized program flow for the Rx-DSP assembly code. Dashed lines indicate command/control flow, while solid lines include data as well. Color backgrounds show which parts of the code run at the given clock rates, with FIFOs and wait cycles allowing for asynchronous operation. The two callout boxes show modularized routines in the codebase, some, all, or none of which may be used by a given ARC.

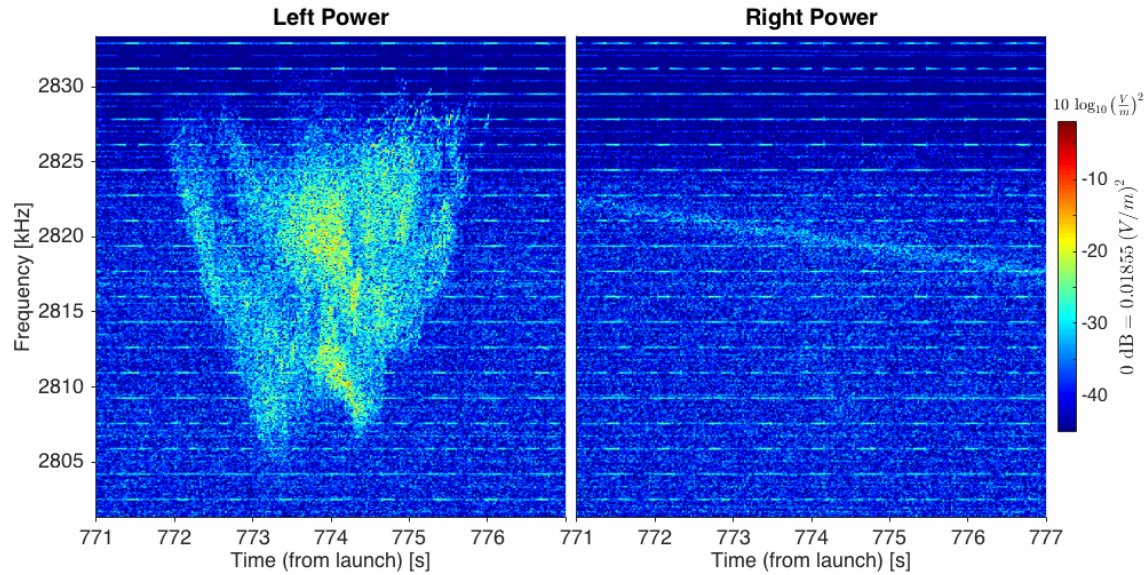


Figure 4. Power spectra of Rx-DSP data from CHARM II, recombined to yield left- and right-circularly polarized powers. The line of power with decreasing frequency seen in the righthand plot is an interference line of unknown origin which exists through much of the flight, and has been seen on other flights.

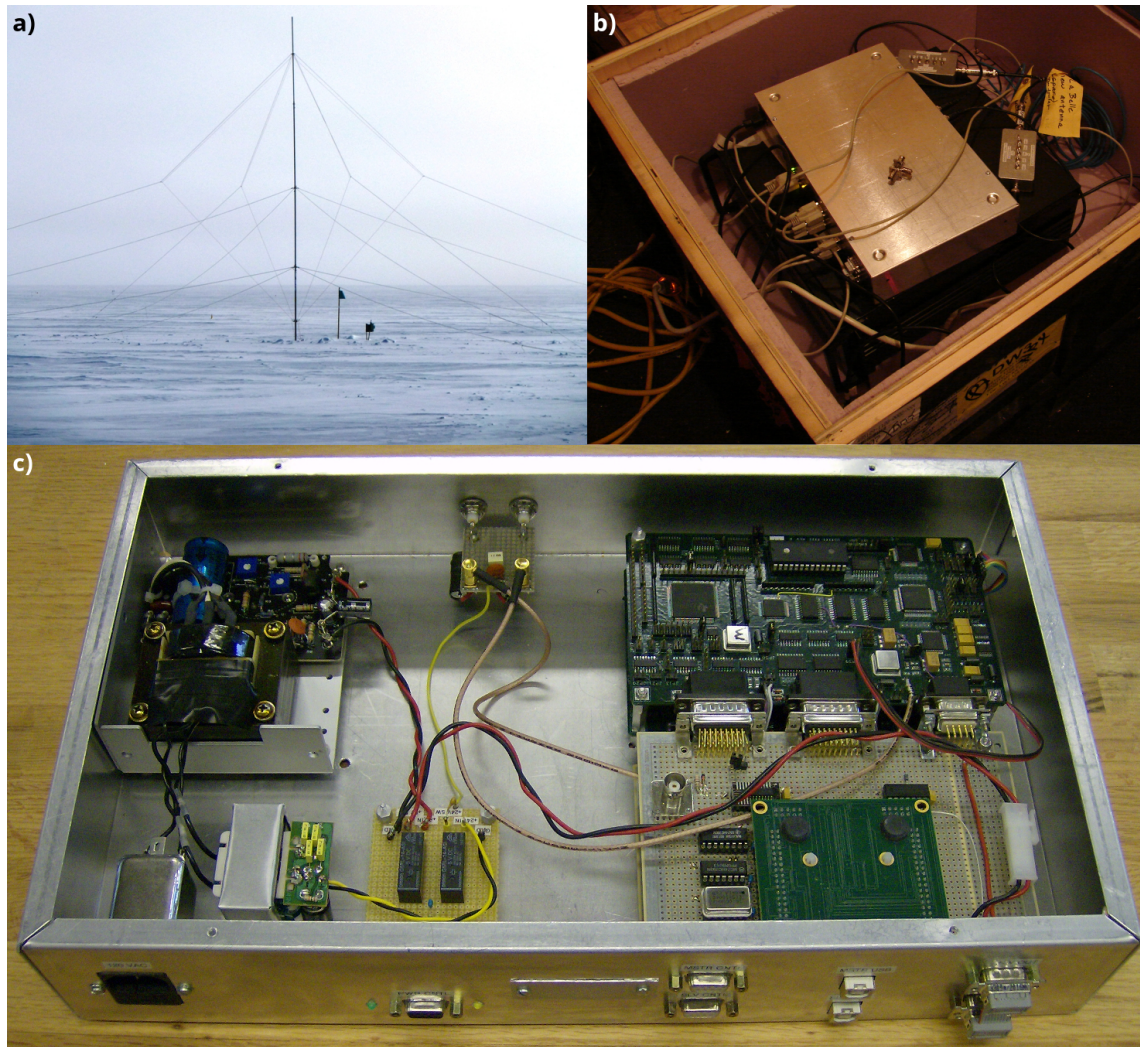


Figure 5. Photos of the various components of the South Pole Station PF-ARC. Top left shows the crossed-loop antenna with a 30 ft mast, and the pre-amplifier at the base. Top right shows the receiver box, data-acquisition PC, and various other equipment within an insulated box (covered when in operation). Bottom shows a lab-bench photo of a PF-ARC, with two vertically stacked, sample-synchronized Rx-DSP boards and adjoined QuickUSB breakout boards on the right side.

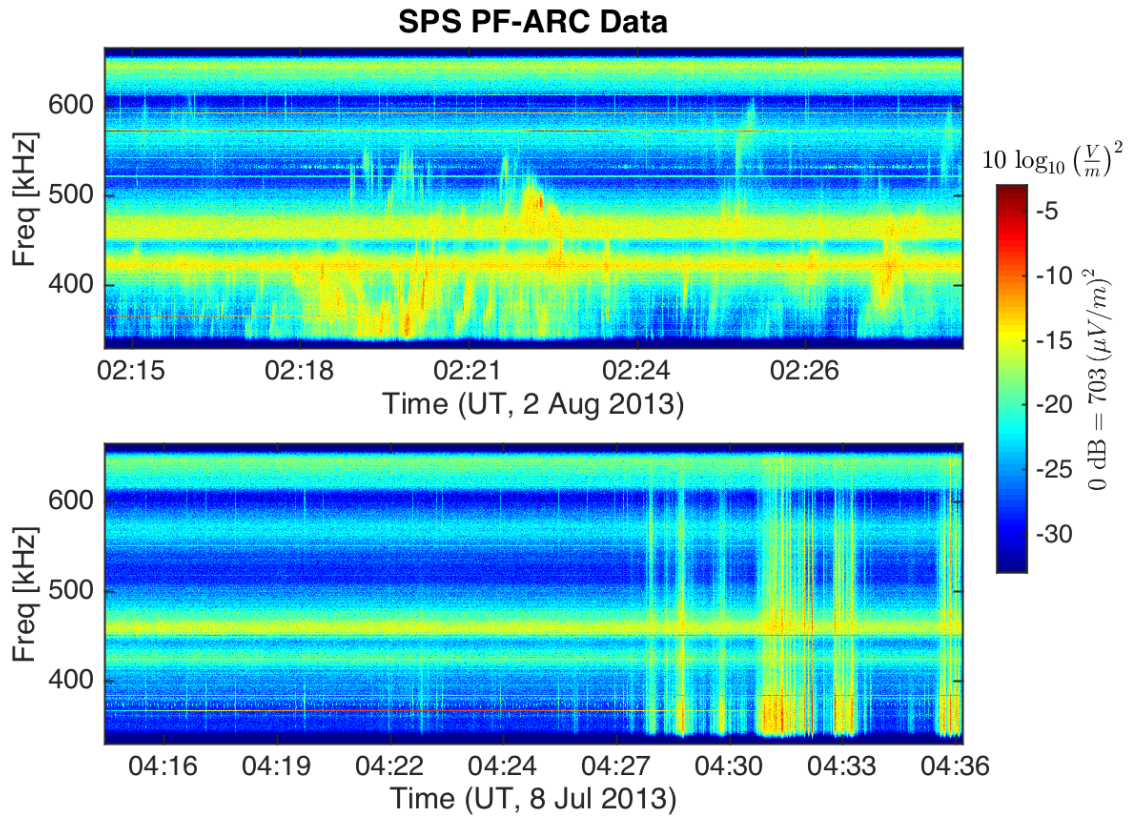


Figure 6. Results from the PF-ARC at South Pole Station. The upper spectrogram shows fine structures in signals which appear similar to Auroral Kilometric Radiation, while the lower plot shows an example of auroral hiss, for comparison.

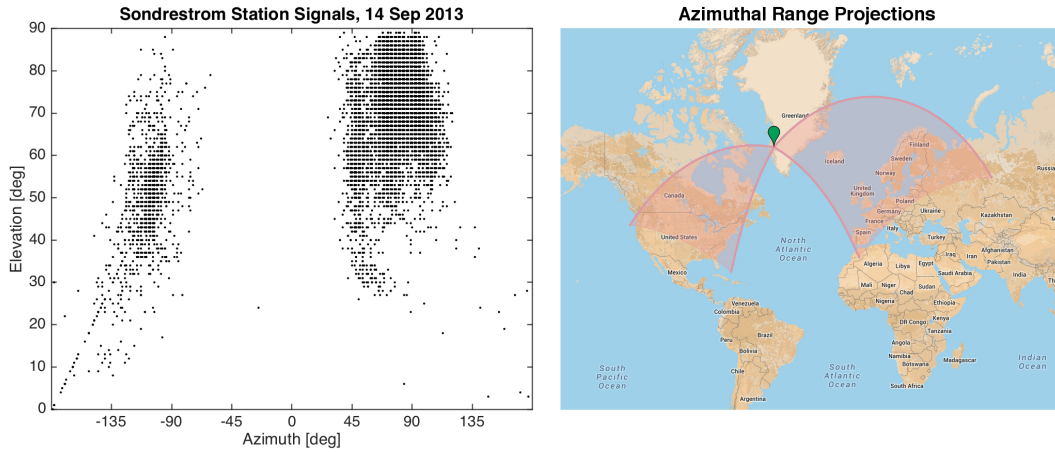


Figure 7. Proof of functionality for the MI-ARC at Sondrestrom Station. To the left, an elevation vs. azimuth scatter plot (elevation from the horizon, azimuth in degrees from true north) of high-coherence points for 14 Sep 2013, showing two clear clusters of points. To the right, we project the azimuthal ranges of the two clusters onto a map, implying that the clusters correspond to signals transmitted from Europe and North America [Map data ©2015 Google, INEGI].